The influence of oblique waves on the azimuthal response of a Ku-band scatterometer: a laboratory study

Nicolas Reul, Hubert Branger, Larry Bliven, Jean-Paul Giovanangeli

The Influence of Oblique Waves on the Azimuthal Response of a Ku-band Scatterometer: A Laboratory Study

Nicolas Reul, Hubert Branger, Larry F. Bliven, and Jean-Paul Giovanangeli

***Abstract*— We conducted experiments in the large wind-wave tank at IRPHE[1] to examine the influence of longer waves propagating at oblique angles to the wind direction on microwave backscattering. Measurements were made of wind, wave directional spectra, and cross sections from a 13.5-GHz scatterometer at 30° from nadir incidence angle. We characterize the scatterometric azimuthal scans with respect to the magnitude and the direction of the maximum backscattered power. Scans of solely wind waves are used to assess the effects of oblique waves, for which the scans yield trends that are related to the oblique-wave direction relative to the wind and the oblique-wave steepness. In particular, cross-section maxima are enhanced by oblique waves and the direction of maxima rotates from the wind axis toward the oblique-wave direction. These scatterometer data, in addition to other oblique-wave studies, led us to conclude that wind vectors produced from standard retrieval algorithms for scatterometers should be used with prudence in regions with significant veering winds, such as near meteorological fronts.**

***Index Terms*— Azimuthal response, oblique waves, scatterometer, sea surface.**

I. Introduction

THE RELATIONSHIP between radar backscattering from the ocean surface and the wind vector is interesting and informative, and scatterometer data can be obtained locally from airborne radars and globally from spaceborne radars. Wind vectors derived by spaceborne scatterometers are important for weather and climate studies as well as for sea-state assessment and oceanic circulation modeling. In spite of recent advances, theoretical models are not yet sufficiently robust to adequately infer surface winds from radar returns from the ocean surface for all weather conditions. On the other hand, empirical relationships are also evolving; new ones are developed based upon the preeminent data from observations or models (see, for example, Nghiem *et al.* [1], Colton *et al.* [2], Stoffelen *et al.* [3], Weissman *et al.* [4], and Elfouhaily [5]). So our understanding of the relationship between radar returns from the ocean surface and the wind vector continues to be improved.

Azimuthal scans of scatterometer returns from seas generated by a steady wind have a recognizable shape. For incidence angles between about 30 to 60° from nadir, the scans display the following features: maxima close to the upwind and downwind directions, minima in the crosswind directions, slightly larger values to the upwind direction compared to the downwind direction, and stronger returns with increasing wind speed. These features are often depicted by a three-term cosine model (Moore and Fung [6]), i.e.,

$$\sigma_o(\varphi) = A + B\cos(\varphi) + C\cos(2\varphi) \tag{1}$$

where A, B, and C coefficients are functions of incidence, wind speed, and radar polarization and φ is the azimuthal angle between wind direction and radar-looking direction. This formulation is widely used to infer wind vectors from satellite scatterometers ([7]). Offiler [8] reports that when the dominant longwaves are aligned with the wind direction, the model developed by Stoffelen and Anderson [9] for the ERS-1 C-band scatterometer agrees to 1.5 m·s^{-1} and 8° rms precision with field measurements for neutral stability conditions. Although these results are better than the ERS-1 prelaunch specifications, the quality of wind retrieval estimates could be improved so that new models emerge from time to time (see, for example, [3]).

Wind-generated seas sometimes have waves traveling at considerable angle to the wind direction. There is increasing evidence that the effects of oblique waves, which are longwaves that are not aligned with the wind axis, can be significant for both air–sea interaction processes and inferring winds by remote-sensing techniques. Oblique waves occur during nonstationary weather conditions, like *veering winds*. By veering winds, we mean that the wind direction changes by a significant amount in an interval that is short compared to that required for complete angular relaxation of the waves. With notable gradients near meteorological fronts and major cyclones, short waves rapidly adjust to the local wind conditions but the relaxation time for longwaves is prolonged. Longwaves traveling oblique to the direction of the wind are then observed. Oblique longwave systems can also been observed due to refraction of waves in progressively shallowing

N. Reul, H. Branger, and J.-P. Giovanangeli are with the Laboratoire Océan-atmosphère, Parc Scientifique de Luminy, Institut de Recherche sur les Phénomènes Hors Equilibre, 13288 Marseille Cedex 9, France (e-mail: nicolas@pollux.univ-mrs.fr).

L. F. Bliven is with the Laboratory for Hydrospheric Process, NASA Goddard Space Flight Center, Wallops Flight Facility, Wallops Island, VA 23337 USA.

[1] Previously, IMST (Institut de Mé canique Statistique de la Turbulence).

water. Such situations will tend to *swing* the longwave crests to an alignment parallel to the depth contours. A lateral shear in a current can also refract longwaves, i.e., change their direction of propagation with regards to the wind direction. One aspect of the problems concerns the relationship between the wind and the shortwaves. Several studies (Geernaert *et al.* [10], Rieder *et al.* [11], and Giovanangeli *et al.* [12]) report that in the presence of oblique waves, the direction of the wind-stress vector is not aligned with the wind axis. Hence, the shortwaves should not be symmetrically distributed about the mean wind axis. Scatterometer returns are closely related to shortwave characteristics, so in the presence of oblique waves, application of (1) could produce unreliable estimates of the wind vector. Another aspect of the problem concerns inferring winds using scatterometers. Numerical simulations by Bliven *et al.* [13] show that the azimuthal response of C- and Ku-band scatterometers is significantly modified by the tilt effects associated with oblique waves. Donelan and Pierson [14] reported that there is poor agreement between some azimuthal plots of aircraft scatterometric data and (1); they conjectured that the differences were due to the effects of oblique waves. Likewise, Hauser [15] observed a shift of σ_o-maximum in veering wind conditions during the SEMAPHORE campaign. Stoffelen and Anderson [3] noted that the automatic ERS-1 quality control rejects σ_o triplets from the ERS-1 scatterometer in geophysical situations in which waves are not in equilibrium with the wind. To understand the effects of oblique waves, it would be helpful to have simultaneous measurements of wind, sea-state, and scatterometer response. Unfortunately, there is a dearth of field measurements, so the modification of scatterometric scans by oblique waves remains an open problem.

Wind-wave facilities have been extensively used in studies of air–sea and wave-wave interactions [16]–[22]. Further, wind-wave tanks have a long history in the experimental determination of radar backscatter from the water surface [23]–[29]. Wave-tank experiments provide the possibility of measuring precisely and under controlling the physical parameters of interest: azimuthal radar cross section, directional wind, and wave measurements. Motivated by the successful laboratory measurements of scatterometric scans by Giovanangeli *et al.* [26], the goal of this study is to characterize scans from a Ku-band scatterometer in the presence of oblique waves. The length scale of oblique waves in wind-wave tanks is certainly much smaller than would be observed *in situ*. Still, it is instructive to examine the influence of paddle-generated waves, which are as follows:

1) much longer than Bragg waves;
2) longer than the dominant wind waves;
3) propagating at oblique angles to the wind direction.

II. Experimental Setting

A. Wind-Wave Tank

The experiments were conducted at IRPHE in the large wind-wave tank,[2] which has been described by Coantic and Favre [30] and Coantic *et al.* [18]. The water section is 40 m long, 3 m wide, and 1 m deep; the air-column height is about 1.5 m, and the maximum wind velocity is 14 m·s^{-1}. Fig. 1 shows the general configuration for these experiments.

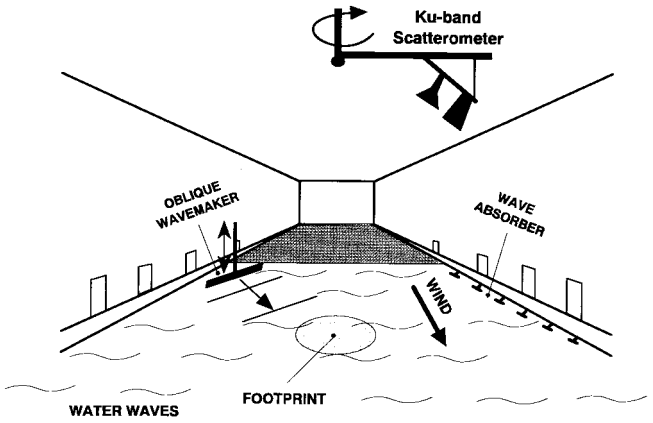

Fig. 1. Experimental arrangement.

In order to create oblique longwaves, an electromechanical plunging wavemaker was installed on one side of the tank. This paddle was a wedge-shaped wavemaker of 1 m long with a width of 10 cm and a height of 15 cm. The amplitude, frequency, and direction of propagation of the longwave system with regard to the wind direction were adjustable. Wave absorbers were located on the sidewall of the tank to avoid parasitical reflection of oblique paddle-waves. The directional spectra of studied wave fields, which are further shown in Section III, clearly demonstrate the efficiency of the oblique wave absorbers. No parasitical reflected waves appear on the spectra. The water surface was cleaned before each experiment by blowing wind so that any surface film collected on a filter at the end of the tank. We obtained data for assorted sea-states with various wind speeds and longwaves. The wind and wave directions are as follows. 0° is the downwind direction and the mean direction of the wind waves, -90 and 90° are the left and right crosswind directions, and $\pm 180°$ is the upwind direction.

Air flow and wind stress are changed slightly by the presence of the wavemaker apparatus in the tank. In a study of the effect of oblique waves on wind stress at IRPHE, Giovanangeli *et al.* [12] made measurements with and without the wavemaker in the wind-wave tank. Their data from the experimental site show that friction velocity increased by less than 10% in intensity and changed by less than 2% in direction. Because the oblique wavemaker was always in the tank during this study, the wind field is comparable for cases with and without oblique waves. Hence, the perturbation of the wind field by the wavemaker is not significant.

In situ oblique waves are much longer than, not only the Bragg waves, but the dominant wind waves. For simulations, however, the maximum wavelength of oblique waves was limited by the width of the tank. Therefore, to restrict the wavelength of wind waves, we devised an artificially short fetch by placing a plastic sheet on the water surface upwind of the measurement site. Because there was limited contact between the wind and the water surface in the upwind direction, the effective fetch was 2.5 m; so for winds up to 10.5 m·s^{-1}, the wavelength of the dominant wind waves was less

[2] Previously, IMST wind-wave tank.

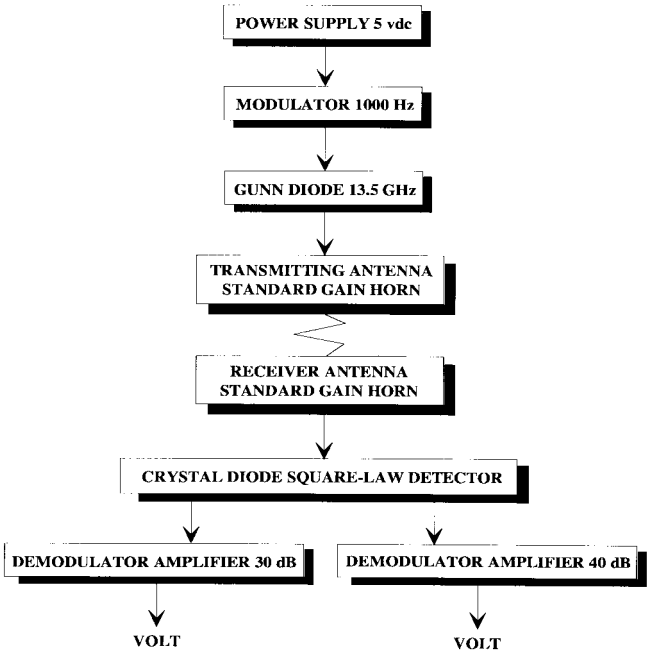

Fig. 2. Radar design.

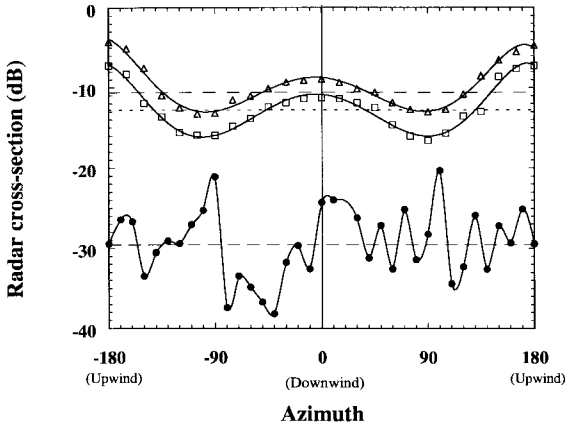

Fig. 3. σ_o azimuthal variations for a calm sea-surface (solid circles), for a 8-m·s^{-1} pure wind-wave field (open squares) and for a 10.5-m·s^{-1} pure wind-wave field (open triangles). Horizontal lines represent the azimuthally averaged backscattered power for each case.

than 16 cm. Thus, the wavelength of the oblique waves was at least three times longer than the dominant wind waves and 20 times longer than the Bragg wavelength.

B. Scatterometer System

The Ku-band scatterometer at IRPHE is a 13.5-GHz (2.2-cm wavelength) system that was operated with vertical polarization and at 30° from nadir incidence angle. This system is like the one developed by Bliven and Norcross [31], which has been used in wave-tanks by Giovanangeli *et al.* [26] at moderate incidence angle and by Branger *et al.* [32] at low incidence angle. A schematic of the radar system is presented in Fig. 2. We used a standard procedure [33] to calibrate the radar. Radar data were normalized by the voltage from a 15-cm diameter metal sphere at 1-m range, which was the distance between the scatterometer and the calm water. We used a mechanical device to alter the azimuthal angle between wind direction and radar observation, while keeping constant the incidence angle and the location of the footprint. The energy coming from the standard gain horn has a relatively narrow beamwidth, i.e., a −3-dB attenuation at 5 and −5° and a −10-dB attenuation at 8 and −8°. The two sidelobes are centered around 14 and −14°, and their relative level is −15 dB. The radar footprint diameter measured at the two-way 3-dB point and at the 1-m range to a calm water surface was approximately elliptical with dimensions of 20 × 17 cm^2.

We performed tests to ensure that σ_o was not adversely affected by scattering from undesirable targets within the tank. Radar absorbing material was installed at appropriate locations around and above the radar setup to minimize multipath reflections. The Eccosorb flat-sheet resonant absorbers reflect −20 dB or less of normally incident microwave energy in the Ku-band. Absorbing panels were suspended from the roof, back, and sides of the tank. A reliable way to measure the degree of noise and ensure that data were not biased by unwanted reflections was to conduct azimuthal response tests for a calm water surface and pure wind-wave fields. Fig. 3 displays the azimuthal variation of the normalized radar cross section for a calm water surface and wind-generated waves at wind speed of 8 m·s^{-1} and 10.5 m·s^{-1}. In spite of the absorbing panels, the radar response from the calm water surface presents two maxima at ±90°: the multipath reflection is maximum when the radar looks at the left and right windows located at the sidewalls and alongside wharfs. We can observe that the mean noise level is approximately −29.5 dB and the mean azimuthal backscattered power is −12.9 dB for a wind blowing at 8 m·s^{-1}, and −10.5 dB for a 10.5-m·s^{-1} wind speed. Thus, the signal-to-noise ratio is found to be satisfactory. The basic azimuthal properties of σ_o reviewed in the introduction (i.e., a quasisinusoidal shape, maxima upwind and downwind, and minima crosswind with an upwind/downwind asymmetry) are observed for both pure wind-wave cases, thus giving clear evidence of the reliability of radar measurements. So unwanted microwave reflections have been minimized. Nevertheless, during the experiments, we chose the strongest wind speed tested, i.e., 10.5 m·s^{-1}, to be completely sure that σ_o was well above the noise level.

Wind field and surface stress might be perturbed by the radar apparatus, and this might cause problems, particularly when the radar is looking downwind, because then the antennas are located upwind of the footprint. However, Giovanangeli *et al.* [26] used a similar rotating scatterometer system to study the azimuthal radar cross section as a function of friction velocity, and they found no significative change in wind field and air flow due to the radar apparatus. The radar structure has little effect on the wind field at the measurement site.

For each azimuthal direction, the backscattered power was recorded at 100 Hz for 120 s. This corresponds to approximately 200 oblique waves, so average cross sections provide reliable estimates of mean values.

C. Wave Measurement Systems

Directional features of the wave field were determined by two different methods, one for frequency domain data and another for wavenumber domain data.

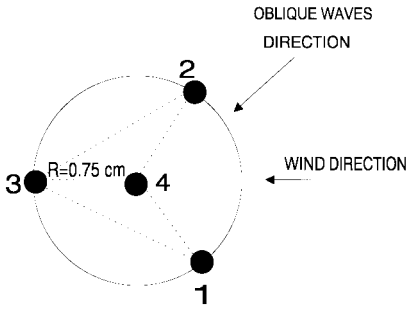

Fig. 4. Wavestaff array configuration seen from above.

1) Frequency Domain Measurement System: We used an array of four capacitance wave gauges (Fig. 4) to measure surface elevation in the frequency domain. These data were processed with a maximum likelihood method (MLM) (Davis and Regier [34]) to obtain directional spectra. The MLM is known to have a high-resolution power for estimating the directional wave spectrum [35]–[37]. To avoid electromagnetic interferences between the probes array and the radar beam, the array was attached to a cart on rails. Before each azimuthal radar measurement, the wavestaffs were brought at the footprint location to measure surface elevations during 230 s at a frequency of 100 Hz and filtered at 50 Hz by a Rockland 852 analog low-pass filter, and then removed out of the radar-looking area without changing waves and wind conditions. The cross spectra were calculated based on blocks of 2048 points, and the MLM was employed with 1° directional spacing.

2) Wavenumber Domain Measurement System: The dispersion relationship for gravity-capillary waves riding on longer waves yields to multiple solutions when transforming from frequency to wavenumber, but not the reverse. So, an optical refraction technique was used to measure waves in the wavenumber domain. This method has been employed by Jähne and Riemer [38], Van Haselma *et al.* [39], Jähne and Schultz [40], Beyer *et al.* [22], and Keller *et al.* [29]. A submerged illumination system similar to the device constructed by Jähne and Riemer [38], and illustrated in Fig. 5(a), is used. The scheme operates on the principle whereby light from a light source with a known spatial gradient under the water is refracted at the water surface and collected by a sensor located above the water. The light source consists of a row of six 150-W Osram HQI metal vapor lamps, which are located at the upwind sidewalls of a 1.4 × 1.4 × 0.3-m^3 plexiglas diffusor box. Each lamp has a brightness efficiency of 75 lm/W. The box contains an aqueous suspension of unisphere latex polystyrene particles used to scatter the light with an exponential attenuation in the uptank/downtank direction. The illumination system is submerged at a depth of 60 cm under the mean water level at the measurement site and does not cause any disturbance of the flow and waves in the water tank. The sensor used to collect images is a CCD camera located 1.5 m above the water, and it looks downward at the water surface. Images were digitized (512 × 512 pixels) by an 8-bit video frame data acquisition card in a PC computer. Since a full frame consists

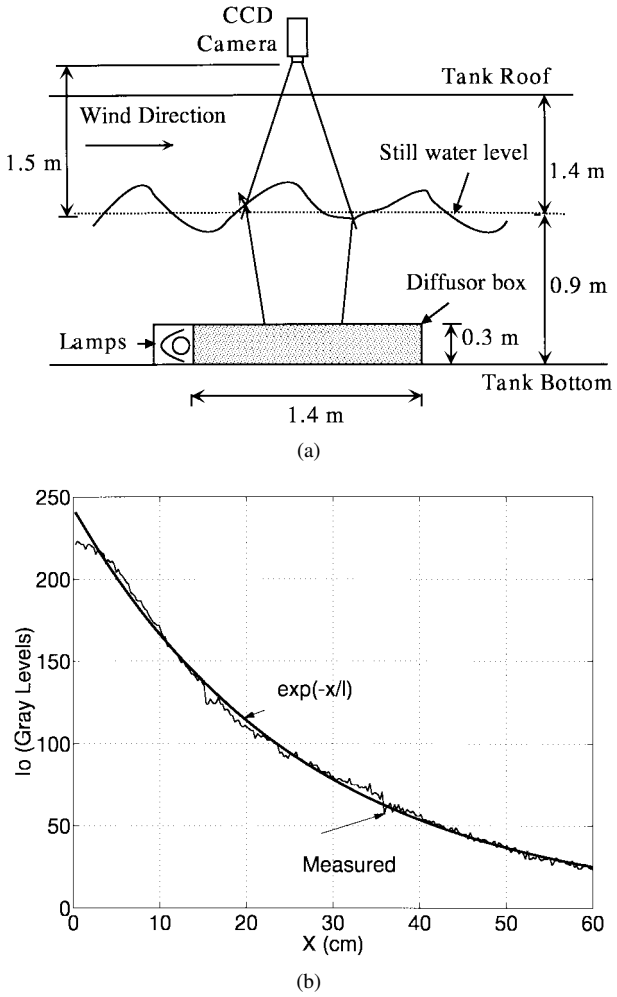

Fig. 5. (a) Optical system. (b) Comparison of measured and fitted light intensity in the uptank/downtank direction from a CCD image of still water.

of two half frames that are individually illuminated with a time difference of 20 ms, only half frames with an along-wind and crosswind resolution of 256 and 512 pixels, respectively, were processed. An approximation of the along-wind component of the wave-slope S_X at a given point (x, y) can be retrieved with a simple geometric law (Jähne and Riemer [38]), a function of the brightness of the image with the waves I_W and the brightness of the image of the flat surface I_0

$$S_X(x,y) = \alpha\left[1 - \frac{I_W(x,y)}{I_0(x,y)}\right] \tag{2}$$

where α is function of the mean water level and the light exponential intensity gradient of I_0. The quantity $S_X(x, y)$ is preconditioned by applying successive image processing to the data. A 3 × 3 median filter was used to reduced efficiently the noise level introduced by the acquisition devices. Evidence for the accurate exponential nature of the scattering is shown in Fig. 5(b), where an uptank/downtank cut through the CCD image is compared with an e-folding scattering length l of 26.5 cm. But very close to the light source, the light scattering is not exponential, as can be seen in the first five centimeters of Fig. 5(b), and far from the light source, the camera is not sensitive enough to detect a significative decay of light

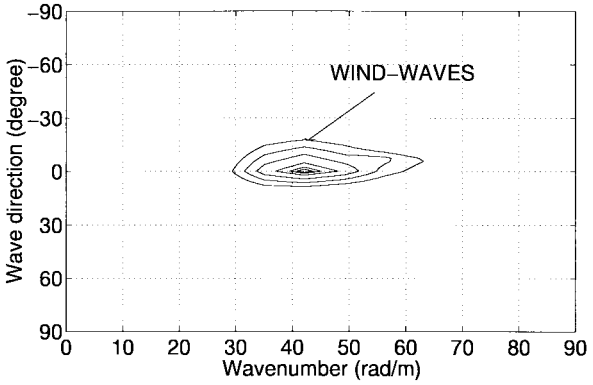

Fig. 6. Contour plots of the directional wave-slope wavenumber spectrum of a 10.5-m·s^{-1} pure wind-wave field. 0° corresponds to the wave-tank main direction. Negative angle values correspond to waves propagating to the left of the mean wind axis and positive values to the right. The increment between two lines is one seventh of the spectrum maximum value.

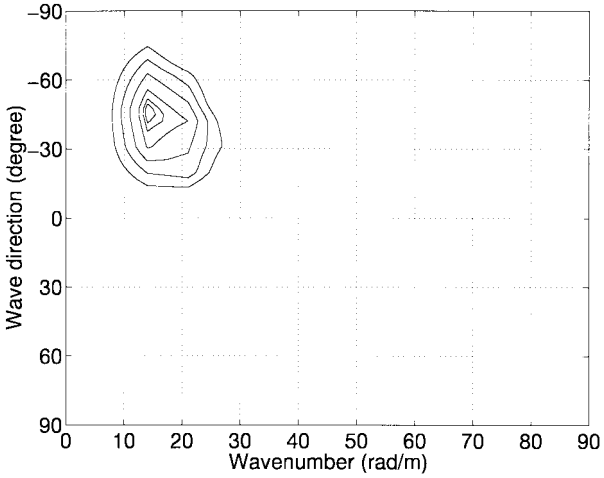

Fig. 7. Contour plot of the directional wave-slope wavenumber spectrum of along-wave system propagating at −45° from the wave-tank main direction. Negative angle values correspond to waves propagating to the left of the main wave-tank axis. The increment between two lines is one-seventh of the spectrum maximum value.

intensity. In order to avoid these spurious effects, the analysis is constrained to 55-cm up/downwind and 70-cm crosswind. Each image was fitted by a plane with a least-squares algorithm. The fitted plane was subtracted from the image to avoid spectral leakage into the low wavenumber range due to waves with wavelengths larger than the imaged sector. A two-dimensional (2-D) Hanning window was then applied to the images. Directional wave slope spectra were then computed by 2-D fast Fourier transform (FFT) of $S_X(x, y)$ and averaged over 16 images. Geometric calibrations of the imaging slope gauge were performed by floating on the water an artificial transparent plastic wave. This calibration wave consisted of a sinusoidal wave with a wavelength of 10 cm and a steepness $ak = 1.16$. The plastic wave was orientated in several directions on the water surface to determine the accuracy of the measurements. The optical system provided information on all scales of the wind waves, down to about 15 cm^{-1} in wavenumber and with an rms accuracy of 3^{circ} in direction. Since the Bragg waves for the Ku-band scatterometer were at 2.9 cm^{-1}, they were detectable with the optical system. Additionally, due to the experimental geometry (illuminated box size, water depth, and the distance between the camera and the water level), waves with slope angle larger than 50° could not be resolved; however, waves rarely exceed this limit.

III. Experimental Results

We use solely wind waves as the basis for assessing the effects of oblique longwaves. The following synopsis of the measurements shows that oblique waves enhance backscatter power and rotate the maxima toward the oblique-wave direction (away from the upwind/downwind direction). Furthermore, the magnitude of these effects varies with respect to oblique-wave incidence angle and oblique-wave steepness.

A. Baseline Conditions

We used a solely wind case of 10.5 m·s^{-1} to obtain a wind-wave spectrum and scatterometer scan for a typical wave condition. The corresponding directional slope spectrum is shown in Fig. 6. Since wavenumber $k = 2\pi/\lambda$, where λ is the wavelength, the dominant wavelength is approximately 15 cm and the maximum of the spectrum is aligned with the wind direction. We do not see anomalies due to the oblique wavemaker that was upwind of the measurement site. The associated scatterometer scan is displayed in Fig. 3, which shows that the mean backscattered power is significantly higher than that from a calm sea surface. The scan does not show any peculiarities due to the presence of the oblique wave generator; indeed, the scatterometer scan appears to be quite normal (cf., Section II-B). The 10.5-m·s^{-1} solely wind case provides a suitable baseline condition to assess the effects of oblique paddle-generated longwaves.

B. On the Influence of Oblique Waves

We first acquired data from an oblique paddle-generated wave case without wind to characterize the radar response from pure oblique waves. Fig. 7 shows a contour plot of the directional wave-slope wavenumber spectrum. The peak wavelength is 45 cm ($k \sim 14$ rad·m^{-1}), the steepness is $\epsilon = ak \sim 0.12$, and the oblique-wave incidence angle is −45° (counterclockwise and relative to the upwind direction). Because the oblique waves are effectively attenuated by the wave absorbers on the sidewalls, no secondary peak from eventual reflected waves appears on the directional wavenumber spectrum.

Fig. 8 shows the scatscan, which is somewhat elevated compared to the backscattered power level from a calm surface; however, the mean backscattered power from oblique waves is much lower than the mean backscattered power from solely wind waves. The cross sections from oblique waves seem to vary randomly with azimuth, although there are two small maxima near the ±90° directions, where multipath reflection is most difficult to suppress. Kwoh and Lake [41] found that the scatterometer returns from paddle-generated waves are attributable to various processes: specular reflection from turbulent wakes, nonspecular processes like rounded

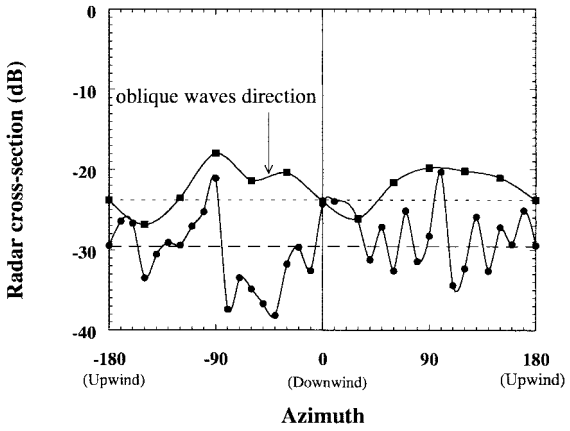

Fig. 8. σ_o azimuthal variations for a calm sea-surface (solid circles) and for a pure mechanically generated oblique wave field (solid squares). The azimuth corresponding to the direction of propagation of long waves is indicated ($-45°$). Horizontal lines represent the azimuthally averaged backscattered power for each case (-24 dB for the pure mechanically generated oblique wave field and -29.5 dB for the noise level).

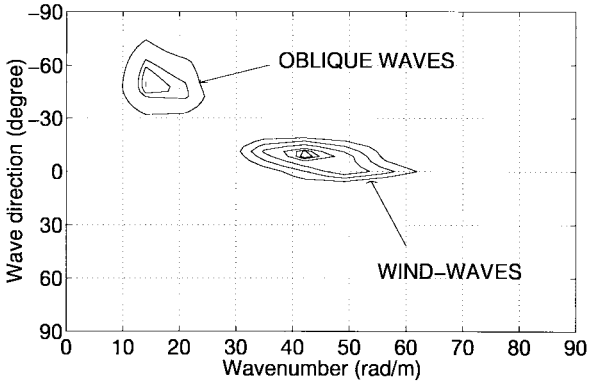

Fig. 9. Contour plots of the directional wave-slope wavenumber spectrum of a a wave field generated by a wind blowing at 10.5 m·s^{-1} accompanied by an oblique longwave system propagating at $-45°$. Negative angle values correspond to waves propagating to the left of the main wave-tank axis and positive values to the right. The increment between two lines is one-seventh of the spectrum maximum value.

wedge diffraction from sharp crests of waves, Bragg scattering from parasitic capillaries, and turbulent patches.

We illustrate the main effects of oblique waves by the combined case of wind waves (10.5-m·s^{-1} wind speed) riding on oblique waves (at $-45°$ from the wind direction). The directional wave-slope wavenumber spectrum for this sea-state is shown in Fig. 9. The wavelength of the dominant wind waves is about 15 cm ($k \sim 42$ rad·m^{-1}), whereas the oblique-wave wavelength is about 45 cm ($k \sim 14$ rad·m^{-1}). The wavelength of the oblique waves is nearly three times longer than the dominant wind-generated waves and nearly 20 times longer than the radar Bragg wavelength. Note here that the peak direction of wind waves is rotated approximately 10° from the wind axis, toward the direction of propagation of the oblique waves. The scatterometer scan is displayed in Fig. 10, which reveals that the oblique waves enhanced the backscatter by as much as 3 dB compared to the wind case. Fig. 10 also shows that the maxima of the oblique wave scan are rotated toward in the oblique wave axis, rather than being

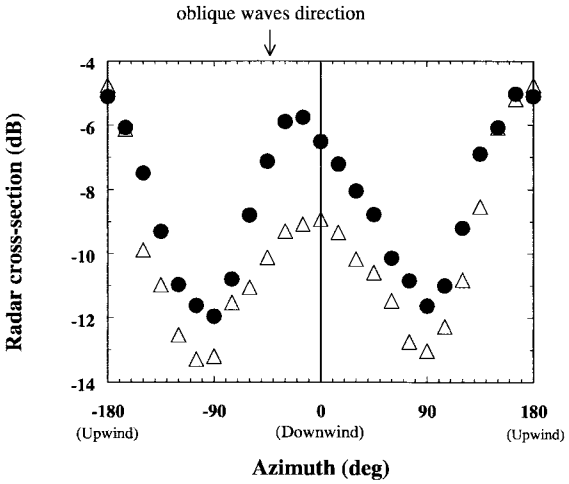

Fig. 10. σ_o azimuthal variations for a 10.5-m·s^{-1} pure wind-wave field (open triangles) and $-45°$ oblique longwave system with a 10.5-m·s^{-1} wind-generated wave field (solid circles).

aligned with the wind axis. The maxima are between the mean wind direction and the direction of the longwave propagation, at approximately half the angle between the oblique-wave direction and the mean wind direction. The influence of the oblique-wave incidence angle and the oblique-wave steepness on the azimuthal radar response is discussed in the next sections.

C. On the Influence of Oblique-Wave Incidence Angle

To assess the influence of oblique-wave incidence angle on abnormal scatterometer returns from the baseline wind case, we acquired data for the oblique waves propagating at -10, -25, and $-45°$ from the wind direction. The oblique-wave steepness was $\epsilon = ak \sim 0.12$. Contour plots of the directional frequency spectra of the surface elevation for these three sea states and for the pure wind-wave case (10.5-m·s^{-1} wind speed) are presented in Fig. 11. All of these spectra show that the wind-wave system is biased toward the direction of the oblique-wave system. The larger the oblique-wave angle, the higher the wind-wave shift. The angular shift increases from about 12° for 25° oblique waves to about 17° for 45° oblique waves.

Fig. 12 is a blow up from crosswind to downwind radar-looking directions of the azimuthal radar response for the four different sea states. We focused our study on this area to obtain a detailed investigation of the azimuthal range, where the shift was expected to occur. Moreover in the downwind direction, the wavemaker setup might not affect radar backscatter. Clearly, the larger the oblique-wave incidence angle, the greater the shift of the σ_o-maximum away from the wind direction. As observed in the previous section, σ_o-maximum lies between the mean wind direction and the direction of propagation of the longwaves. The observed shift angle of the downwind σ_o-maximum $\Delta\varphi$ is plotted in Fig. 13(a) versus the oblique-wave incidence angle θ. The observed angular shift of σ_o-maximum is coherent with the angular shift of the dominant wind waves. The relationship between the angular

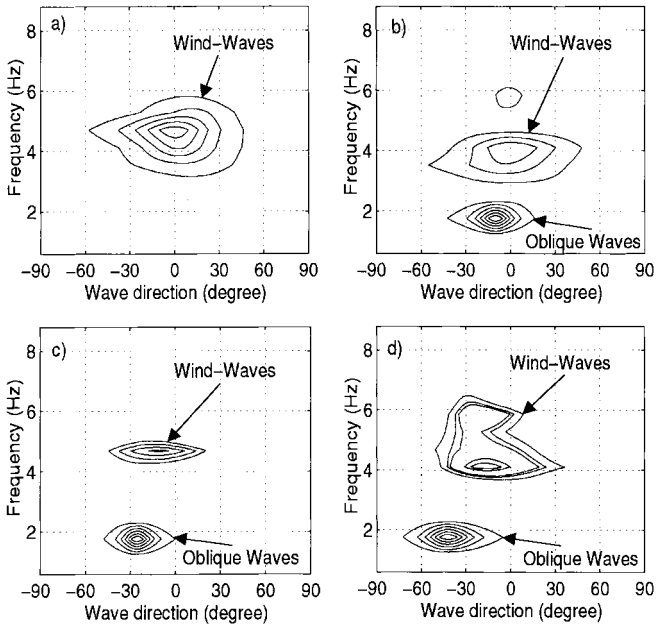

Fig. 11. Contour plots of the directional frequency spectra (a) for a 10.5-m·s^{-1} pure wind-wave field, (b) oblique longwave systems propagating over a 10.5-m·s^{-1} wind-generated wave field with incidence angles of $-10°$, (c) $-25°$, and (d) $-45°$ with regard to the mean wind axis. Negative angle values correspond to waves propagating to the left of the main wave-tank axis and positive values to the right. For each graph, the increment between two lines is one-seventh of the spectrum maximum value.

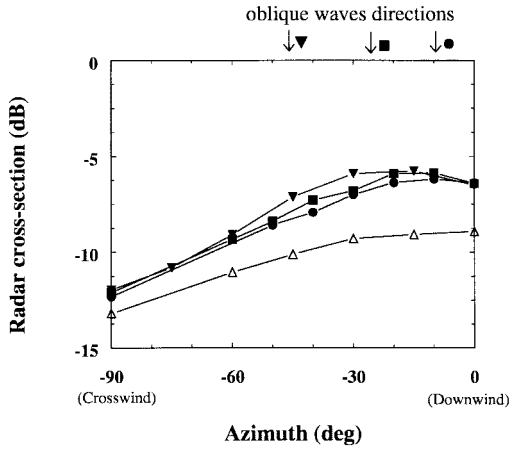

Fig. 12. Azimuthal scans of the Ku-band scatterometer for a 10.5-m·s^{-1} pure wind-wave field (open triangles) and different oblique longwave incidences θ: $-10°$ (solid circles), $-25°$ (solid squares), and $-45°$ (solid triangles). The corresponding oblique longwave directions are indicated. The oblique longwave steepness was kept constant ($\epsilon = ak \sim 0.12$).

dispersion of Bragg waves and the σ_o-maximum deviation will be discussed further in Section IV.

As observed in the previous section, Fig. 12 reveals a significant enhancement of the cross-section σ_o. The difference of backscattered power level $\Delta\sigma_o$ for $\sigma^o_{\max}$ between oblique-wave experiments and the wind-only case is plotted in Fig. 13(b) versus oblique-wave incidence (for a constant wave steepness $\epsilon = ak \sim 0.12$). The larger the oblique-wave incidence angle, the higher the cross section. It might be pointed out that we compare backscattering from a coupled wind-wave/oblique paddle-wave system with backscattering

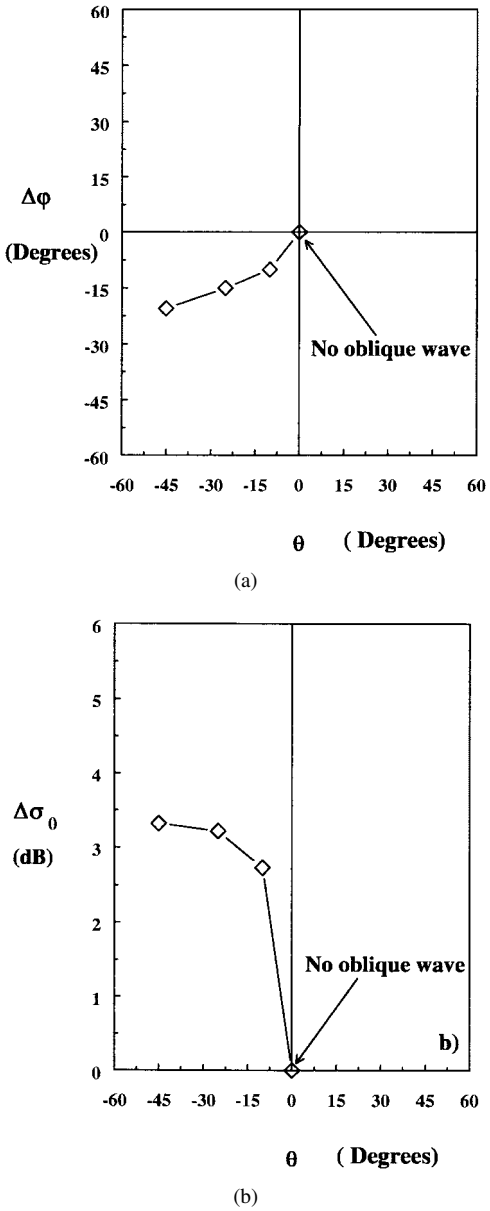

Fig. 13. (a) Shift angle of the downwind σ_o-maximum value $\Delta\varphi$, as a function of longwave incidence angle θ. (b) Difference ($\Delta\sigma_o$) between the downwind σ_o-maximum value in presence of longwaves and without longwaves, as a function of longwave incidence angle θ. The oblique longwave steepness was kept constant ($\epsilon = ak \sim 0.12$).

from a pure wind-wave system. Unfortunately, it has not been possible to generate paddle-waves with 0° incidence angle (i.e., aligned with the wind direction) because, in that case, the wavemaker would have been located just upwind of the measurement area, thus modifying the air flow and wind stress by the turbulent wake of the experimental apparatus.

Fig. 12 also illustrates an increase in the crosswind/downwind asymmetry in the presence of oblique waves.

D. On the Influence of Oblique-Wave Steepness

A second set of azimuthal tests were performed to observe the effects of the longwave steepness on σ_o behavior. Four different oblique longwave steepnesses $\epsilon = ak$ ranging from 0.07 to 0.26 were studied while keeping constant the incidence

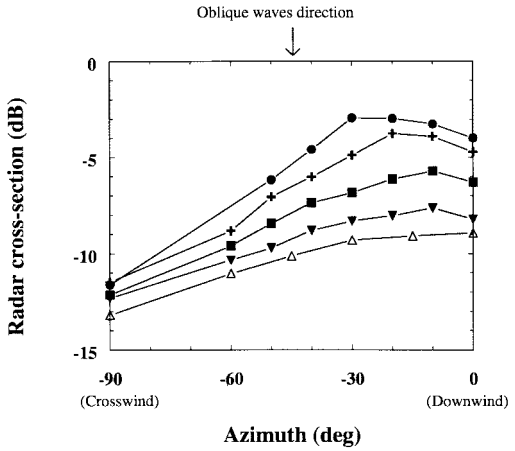

Fig. 14. Azimuthal scans of the radar for different oblique longwave steepnesses: $\epsilon = ak \sim 0.07$ (solid triangles), 0.13 (solid squares), 0.20 (crosses), and 0.26 (solid circles) with a constant longwave incidence angle of $\theta = -45^\circ$ with regard to the mean wind axis. The 10.5-m·s^{-1} wind-only case is also plotted (open triangles).

angle ($-45°$ from the wind direction) and the wind speed (10.5 m·s^{-1}). Fig. 14 represents azimuthal scans of σ_o for these four "sea states." It is obvious that an increase in the oblique-wave steepness yields to the following:

1) increase of the backscattered power (at $\epsilon = ak \sim 0.26$, near the peak, the radar response is 6 dB higher than for the case in which no oblique waves are present);
2) shift of σ_o-maximum toward the direction of propagation of the longwaves;
3) increase in the crosswind/downwind asymmetry.

Points 1) and 2) are illustrated in Fig. 15(a) and (b), where the observed shift angle of the downwind σ_o maximum $\Delta\varphi$ and the increase of backscattered power $\Delta\sigma_o$ are plotted versus the longwave steepness ϵ (for a constant oblique-wave incidence angle $\theta = -45°$).

IV. Discussion

Considering these laboratory results, oblique waves propagating over short wind waves seem to have two main effects on the azimuthal scatterometer response: 1) a shift of the σ_o maximum and 2) an increase of σ_o. This σ_o behavior is probably linked to the spectral modification of the Bragg scatters (2.2-cm wavelength for a 13.5-GHz radar frequency) by the oblique wavetrain, but it may be predominantly due to the tilting effects associated with oblique waves. These points are discussed hereafter

Shift of σ_o Maximum: The shift of σ_o-maximum observed in these wind-wave tank experiments has the same order of magnitude as the shift of σ_o-maximum observed by Hauser [15] during the SEMAPHORE campaign. Likewise, numerical simulations by Bliven *et al.* [13] show that the σ_o-maximum was shifted due to oblique longwaves. One of the physical processes that is responsible for the shift of the maximum of σ_o might be the modification of the Bragg scatters behavior by the oblique wavetrain. These modifications could be due either to *hydrodynamical wave-wave interactions* or *aero-hydrodynamical interactions* between the air flow and the oblique waves.

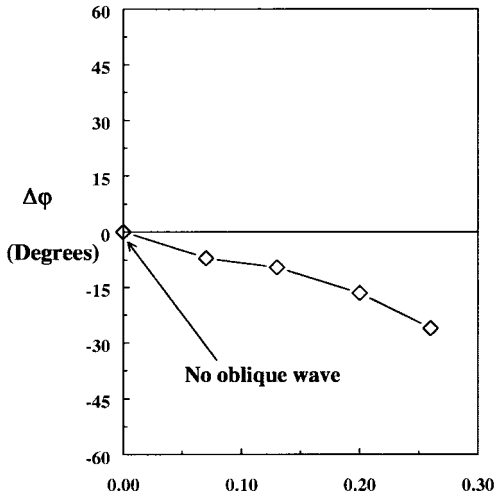

(a)

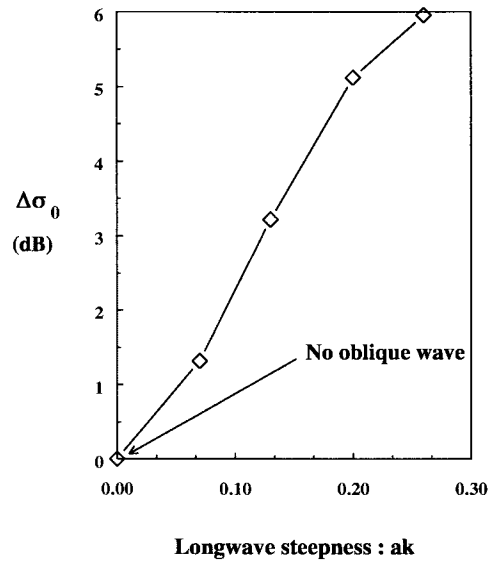

(b)

Fig. 15. (a) Shift angle of the downwind σ_o-maximum, $\Delta\varphi$, as a function of longwave steepness $\epsilon = ak$. (b) Difference ($\Delta\sigma_o$) between the downwind σ_o-maximum value in presence of longwaves and without longwaves, as a function of longwave steepness $\epsilon = ak$. The oblique longwave incidence angle was kept constant ($\theta = -45°$).

An analytical study (Skandrani *et al.* [42]) on the hydrodynamical behavior of short wave trains propagating at a given angle to longwave direction reveals that nonlinear three-dimensional (3-D) interactions between the shortwaves and oblique waves caused by *a shift of the direction of propagation of the shortwaves toward the longwave direction.* This kinematic model considers nonresonant interactions of a linear oblique longwave with nonlinear shortwaves. In this study, Skandrani *et al.* [42] showed that the shift of the shortwaves $\Delta\varphi_{\rm sw}$ was proportional to the longwave steepness $\epsilon_{\rm lw}$ and the oblique longwave incidence angle θ. When the shortwave wavenumber is much greater than the longwave wavenumber $k_{\rm sw} \gg k_{\rm lw}$, then

$$-\tan(\Delta\varphi_{\rm sw}) \sim \beta * \epsilon_{\rm lw}^2 * \cos(2\theta). \qquad (3)$$

β is a complicate nonlinear formulation of the different parameters $k_{\rm lw}$, $k_{\rm sw}$, θ, $\epsilon_{\rm lw}$, and $\epsilon_{\rm sw}$. This relation proves that shortwaves are deflected by longwaves due to nonlinear hydrodynamical wave–wave interactions. The deviation is maximum for $\theta = \pm 45°$, and the higher the longwave steepness $\epsilon_{\rm lw}$, the higher the shift $\Delta\varphi_{\rm sw}$. In our laboratory experiments, $k_{\rm Bragg}/k_{\rm long\text{-}wave} \sim 20$ and the high values of the longwave steepness ($\epsilon_{\rm lw} = ak \sim 0.26$) and the oblique incidence angle ($\theta = -45°$) might explain the significative shift of the direction of the Bragg waves and, consequently, a deviation of the σ_o-maximum.

The 2-D wavenumber spectra given by the optical system allow us to investigate the angular dispersion of the Bragg waves. Fig. 16(a)–(d) show wave spectra as a function of direction at the Bragg wavenumber ($k_{\rm Bragg} = 2.9$ cm^{-1}) for the different longwave incidence cases compared to the pure 10.5-m·s^{-1} wind-wave case. Fig. 16(a) represents two pure 10.5-m·s^{-1} wind-wave cases. The angular dispersion of Bragg waves at this wind speed is almost uniform. As found by others [29], [38], without oblique longwaves and at the wind speed of 10.5 m·s^{-1}, parasitic capillaries have given way to completely disorganized waveforms that almost completely fill the space. In the presence of oblique long waves, it seems that Bragg waves are shifted toward the longwave, as shown in Fig. 16(b)–(d). This is particularly clear for the larger longwaves incidence case [Fig. 16(d)], in which a significant deviation is observed around $-25°$. However, these spectra must be used with care when making such an interpretation because of the low number of available images (16) over which each of them were averaged.

Bragg scatters are strongly related to the wind-stress vector at the surface. Laboratory work [26] and recent open field experiments (Colton *et al.* [2]) suggest that the azimuthal response of a scatterometer is more directly the result of wind stress than wind speed. Thus, the azimuthal radar cross-section behavior could be related to wind-stress vector modifications in the presence of oblique longwaves. Several theoretical and experimental works have been performed on the effect of oblique longwaves on the surface stress vector and shortwave behavior. From an aerodynamical point of view, Townsend [43] derived linearized equations for the mean flow and turbulent stress over sinusoidal traveling surface waves. When the wind blows over oblique longwaves, he found theoretically and numerically that the direction of the stress tensor is shifted toward the oblique waves. The stress deviation is due to the modification by the longwaves of the direction of the vertical gradient of horizontal velocity in the air. Moreover, recent laboratory experiments (Giovanangeli *et al.* [12]) reported that when the wind is blowing over oblique gravity waves, under a critical height above the surface, *the stress vector is shifted toward the longwaves direction* and this shift angle depends strongly on the longwave features (direction of propagation and steepness).

These studies are consistent with the shift angle of the σ_o maximum we observed during the experiments. In conclusion, two effects, which are strongly linked, may explain the observed shift: on the one hand, it seems that the oblique longwave train modifies the hydrodynamical behavior of the short Bragg waves and, particularly, their mean direction of propagation; on the other hand, the flow above water is modified by the oblique waves leading to a turning of the wind-stress vector and, thus, to a turning of the wind-generated Bragg waves. However, while these mechanisms are valid for deviation angle of the σ_o maximum, there are problems with proposing purely spectral explanations for the large enhancement of the cross section.

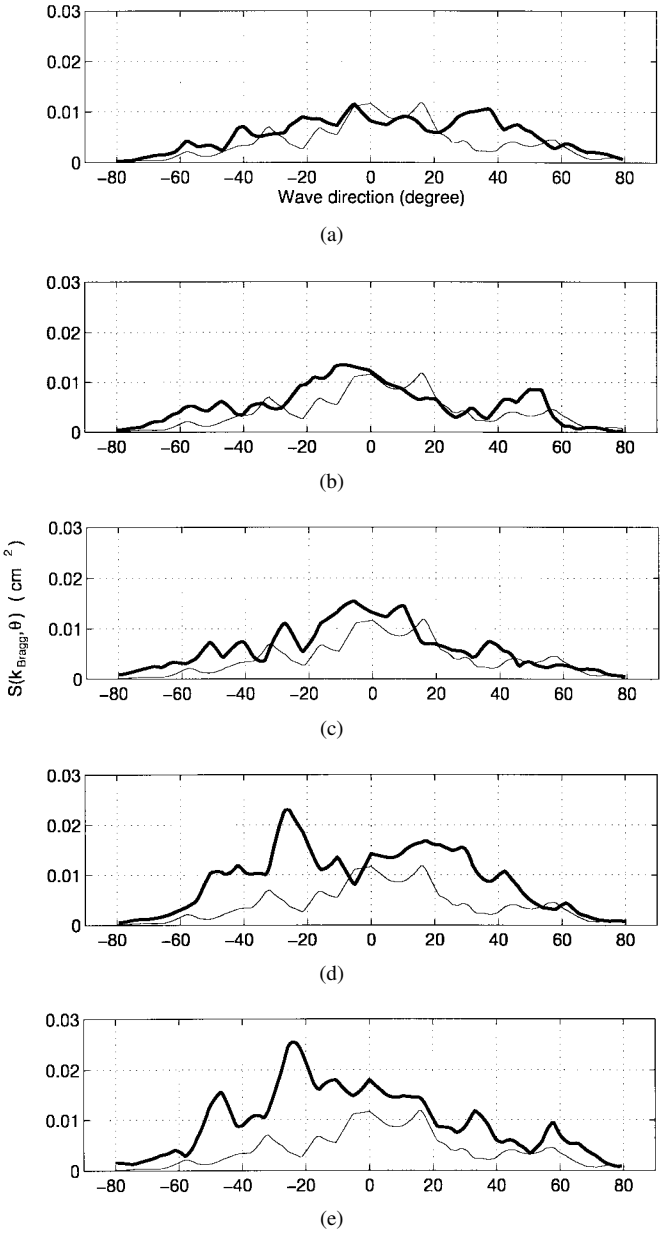

Fig. 16. Evolution of the angular dispersion of Bragg waves as a function of longwave incidence angle and steepness. The thin line is measured Bragg wave spectral data as a function of direction for a pure 10.5-m·s^{-1} wind-wave case. The thick lines represent angular dispersion of Bragg waves for the different following sea-states: (a) another pure 10.5-m·s^{-1} wind-wave case. (b)–(e) wind speed of 10.5 m·s^{-1} and paddle-generated oblique wave train with the following characteristics: (b) steepness $\epsilon = ak \sim 0.12$ and oblique incidence $\theta = -10°$, (c) steepness $\epsilon = ak \sim 0.12$ and oblique incidence $\theta = -25°$, (d) steepness $\epsilon = ak \sim 0.12$ and oblique incidence $\theta = -45°$, and (e) steepness $\epsilon = ak \sim 0.26$ and oblique incidence $\theta = -45°$.

Increase of Backscattered Power Level: A first approach is to compare the energy level of the Bragg frequency component

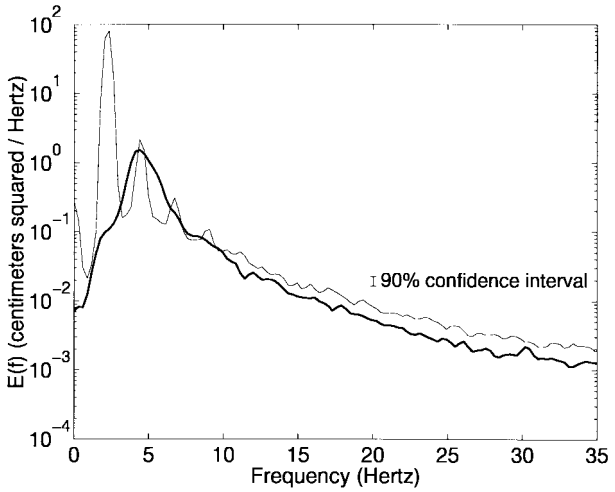

Fig. 17. Evolution of the water elevation power spectra on log-linear scale. The thin line is the spectrum of a paddle-generated oblique wavetrain (steepness $\epsilon = ak \sim 0.26$ and oblique incidence $\theta = -45°$) coupled with a wind speed of 10.5 m·s^{-1}. The thick line corresponds to the water elevation spectrum for the pure 10.5-m·s^{-1} wind-wave case.

of the wave spectrum with and without oblique waves. Fig. 17 shows the power spectra for wind waves only and for wind waves perturbated by an oblique longwave train of steepness $\epsilon = ak \sim 0.26$ and incidence $\theta = -45°$. Looking at the wind $+$ paddle-wave spectrum, it is clear that the spectral density near the peak of the wind waves is narrowed and reduced (except at the longwave first harmonic peak). At higher frequencies, the trend is reversed: in the presence of longwaves, the shortwave energy increases by a factor of approximately two. These results have already been observed by Donelan [44] for a swell traveling in the same direction than the wind. The intrinsic frequency of Bragg wave and the surface drift at a wind speed of about 10.5 ms^{-1} (which, according to Giovanangeli *et al.* [26], corresponds to a friction velocity of 50 cms^{-1}, in the IRPHE large tank) combine for a total frequency of 12.74 Hz. At this frequency, the increase in spectral density is on the order of 1.5 dB. However, this result has to be considered with prudence with regard to the 90% confidence interval of the computed spectrum. Fig. 16(e) show the same order of increase in spectral density around $\theta = -25°$. Yet, the measured cross section under identical conditions, according to Fig. 15(b), increases by 6 dB. It is clear that this large jump in the σ_o is not due only to increased spectral density since, by the Bragg interpretation, the two are directly proportional. Moreover, Fig. 16(d) and (e) reveal that Bragg wave energy stay approximately the same as longwave steepness increases from 0.12 to 0.26. Contrarily, Fig. 15(b) show an increase of 3 dB in the σ_o-maximum. Consequently, other physical mechanisms may be involved in the enhancement of the σ_o.

As stated in Section III-C, it has not been possible to generate paddle waves with 0° incidence angle (i.e., aligned with the wind direction). A possible effect of the paddle wave is to change the effective fetch length due to wave-orbital current interactions at the surface, thus modifying the shortwave generation by the wind and consequently the radar backscatter [45]–[47].

A second idea is to recall that the Bragg mechanism is a resonance phenomenon: to an optical point of view, scatterometers are very sensible to coherent structures of the wave field. Many investigators [48]–[50], [28] reported that quite often the generation of ripples on the front slope of short gravity waves is observed and that these hydrodynamic disturbances act as very coherent sources that produce a strong local microwave power return. Furthermore, it has been observed that the effects of these particular scatters is stronger as the steepness of the gravity waves increases, which is coherent with our results and could explain the increase of σ_o observed in Figs. 13(b) and 15(b).

In addition, at intermediate radar incidence angles, not only the Bragg resonance scattering, but the quasispecular point scattering might contribute to the radar response ([41]). It has been observed that the steeper the short gravity waves, the steeper the ripples are. Consequently, local specular scattering could happened on these steep ripples and produce enhanced level of σ_o. Moreover, at high longwave steepness and with the wind, local wave breaking occurs on the crest of the long waves and might contribute to the observed increase of σ_o (Jessup *et al.* [51], [52]).

Finally, the measurements are more than sufficient to support an interpretation of enhanced σ_o as due to tilting and decreases in the local incidence angle. This is evident in the following two ways.

1) Wavelength of the paddle-generated wave is close to that of the dominant wind-generated wave (15 cm). Keller *et al.* [29] determined that waves of wavelengths greater than $3\lambda_B$, where λ_B is the Bragg wavelength (2.2 cm in our experimental configuration), should be considered as tilting the surface. Thus, both paddle wave and dominant wind wave are sufficiently long in a composite sense to be considered as contributing to the tilting of the surface.
2) Paddle-generated wave is very steep, very small, and, very 3-D relative to the beamspot on the water (20×17 cm as opposed to a wavelength of 45 cm for the paddle wave). The measurements of $\Delta\sigma_o$ in Fig. 15(b) show that the more extreme the steepness, the greater the enhancement of σ_o. At an incidence angle of 30°, it only takes changes of a few degrees to raise the overall σ_o by 3 dB. In the model of Donelan and Pierson [14], a decrease in local incidence angle of 4° at 30° is sufficient to increase σ_o by 3 dB at the wind speed indicated. Assuming a simple double triangular shape for the paddle wave, a steepness of 0.1 corresponds to a decrease in local incidence of 3.6°, and of 0.3 corresponds to 10.8°. For 10.8°, Donelan and Pierson predict increased σ_o of 7 dB, or more than the measured increase of 6 dB.

V. Conclusion

These laboratory data reveal that oblique waves can cause significant changes in cross-section azimuthal scans; i.e., scan averaged power level increases and the alignment of the maxima is skewed away from the wind axis toward the oblique axis. These results are consistent with measurements of wind stress and oblique waves [10]–[12], cross-section

modification by oblique swell [15], numerical simulations of longwave–shortwave interactions [42], tilt effect on scatterometer returns [53] and [13], and the spatial distribution of ERS-1 scatterometer data [3].

When it is difficult to study the effects of natural phenomena, we need to examine the available data and model simulations to assess the need to commit to the demanding task of a definitive investigation. The oblique wave (veering wind) problem certainly is difficult to study. Open field experiments have yet to produce precise simultaneous measurements of the wind speed vector, sea-state and azimuthal scans of cross section; physical constraints inherent in wave-tank studies hamper the simulations; and lack of a complete understanding of physical processes stymies numerical simulations. Nevertheless, we believe that there is sufficient evidence to conclude that oblique longwaves are likely to contribute to errors in both wind speed and direction inferred from inversions of scatterometer azimuthal scans using conventional three-term Fourier models. A coordinated field program is needed to resolve unsettled issues.

ACKNOWLEDGMENT

The authors are very grateful to B. Zucchini and all the technical staff of the IOA-IRPHE laboratory for their diligent laboratory assistance. They especially thank P. Sobieski, who generously loaned the radar absorbing material.

REFERENCES

[1] S. V. Nghiem, F. K. Li, S. Lou, G. Neumann, R. E. McIntosh, C. Carson, J. R. Carswell, E. J. Walsh, M. A. Donelan, and W. M. Drennan, "Observations of radar backscatter at Ku- and C-bands in the presence of large waves during the surface wave dynamics experiment," *IEEE Trans. Geosci. Remote Sensing*, vol. 33, pp. 708–721, May 1995.

[2] M. C. Colton, W. J. Plant, W. C. Keller, and G. L. Geernaert, "Tower-based measurements of normalized radar cross-section from Lake Ontario: Evidence of wind stress dependence," *J. Geophys. Res.*, vol. 100, no. C5, pp. 8791–8813, 1995.

[3] A. Stoffelen and D. Anderson, "The ECMWF contribution to the characterization, interpretation, calibration and validation of ers-1 scatterometer backscatter measurements, and their use in numerical weather prediction models," ECMWF, Shinfield Park, Reading, U.K., ESA Contract Rep. Project 9097/90/nl/bi. 1995.

[4] D. E. Weissman, K. L. Davidson, R. A. Brown, C. A. Friehe, and F. Li, "The relationship between the microwave radar cross section and both wind speed and stress: Model function studies using frontal air-sea experiment data," *J. Geophys. Res.*, vol. 99, no. C5, pp. 10 087–10 108, 1994.

[5] T. M. Elfouhaily, " A consistent wind and wave model and its application to microwave remote sensing of the ocean surface," Ph.D. dissertation, Phys. Dept., Denis Diderot Univ., Paris, France, 1996.

[6] R. K. Moore and A. K. Fung, "Radar determination of winds at sea," *Proc. IEEE*, vol. 67, pp. 1504–1521, Nov. 1979.

[7] A. E. Long, "Toward a C-band radar sea echo model for the ERS-1 scatterometer," in *Int. Conf. Spectral Signatures*, Les Arcs, France, ESA SP-247, 1985.

[8] D. Offiler, "The calibration of ERS-1 satellite scatterometer winds," *J. Atmos. Ocean.*, vol. 11, pp. 1002–1017, 1994.

[9] A. Stoffelen and D. Anderson, "ERS-1 scatterometer data characteristics and wind retrieval skill," in *Proc. 1st ERS-1 Symp.-Space Service Our Environ.*, Cannes, France, 1993, vol. ESA SP-359, pp. 41–48.

[10] G. L. Geernaert, F. Hansen, M. Courtney, and T. Herbers, "Directional attributes of the ocean surface wind-stress vector," *J. Geophys. Res.*, vol. 98, no. C9, pp. 16 571–16 580, 1993.

[11] K. F. Rieder, J. A. Smith, and R. A. Weller, "Observed directional characteristics of the wind, wind-stress and surface waves on the open ocean," *J. Geophys. Res.*, vol. 99, no. C11, pp. 22 589–22 596, 1994.

[12] J.-P. Giovanangeli, F. Remy, and C. Kharif, "A laboratory study of the effect of an oblique swell on wind stress," in *Proc. 2nd Int. Conf. Air–Sea Interaction Meteorol. Oceanogr. Coastal Zone*, Lisbon, Portugal, Sept. 22–27, 1994, vol. 1, p. 297.

[13] L. F. Bliven, V. Billat, P. Sobieski, A. Guissard, H. Branger, and J.-P. Giovanangeli, "An assessment of veering wind effects on scatterometry from the sea-surface," *Int. J. Remote Sensing*, vol. 16, no. 5, pp. 891–898, 1995.

[14] M. A. Donelan and W. J. Pierson, Jr., "Radar scattering and equilibrium ranges in wind-generated waves with application to scatterometry," *J. Geophys. Res.*, vol. 92, no. C5, pp. 4971–5029, 1987.

[15] D. Hauser, "Relationship between the direction of friction velocity and the direction of wind in various sea-state situations observed during the semaphore campaign," in *Proc. 2nd Int. Conf. Air–Sea Interaction Meteorol. Oceanogr. Coastal Zone*, Lisbon, Portugal, Sept. 22–27 1994, vol. 1, pp. 257–258.

[16] J. Wu, "Effects of pulsating wind on velocity profiles and microstructures," *J. Phys. Ocean.,* vol. 5, pp. 782–789, 1975.

[17] E. J. Plate, *Turbulent Fluxes Through the Sea-Surface, Wave Dynamics and Prediction*, A. Favre and K. Hasselmann, Eds. New York: Plenum, 1978.

[18] M. Coantic, A. Ramamonjiarisoa, P. Mestayer, F. Resh, and A. Favre, "Wind-water simulation of small-scale ocean-atmosphere interactions," *J. Geophys. Res.*, vol. 86, no. C7, pp. 6607–6626, 1981.

[19] K. K. Kahma and M. A. Donelan, "A laboratory study of the minimum wind speed for wave generation," *J. Fluid Mech.*, vol. 192, pp. 339–364, 1988.

[20] H. Kawamura and Y. Toba, "Ordered motion in the turbulent boundary layer over wind waves," *J. Fluid Mech.*, vol. 197, pp. 105–138, 1988.

[21] M. L. Banner, "Equilibrium spectra of wind waves," *J. Phys. Oceanogr.*, vol. 20, pp. 966–984, 1990.

[22] M. Beyer, B. Jahne, and W. K. Melville, "Laboratory studies of longwave/short-wave interaction using wavelet analysis of space-time images," in *Proc. 2nd Int. Conf. Air–Sea Interaction Meteorol. Oceanogr. Coastal Zone*, Lisbon, Portugal, Sept. 22–27, 1994, vol. 1, pp. 97–98.

[23] J. W. Wright, "Backscattering from capillary waves with application to sea clutter," *IEEE Trans. Antennas Propagat.*, vol. 14, pp. 749–754, June 1966.

[24] T. R. Larson and J. W. Wright, "Wind-generated gravity capillary waves: Laboratory measurements of temporal growth rates using microwave backscatter," *J. Fluid Mech.*, vol. 70, pp. 417–436, 1975.

[25] W. J. Plant, "A two-scale model of short wind-generated waves and scatterometry," *J. Geophys. Res.*, vol. 91, no. C9, pp. 10 735–10 749, 1986.

[26] J.-P. Giovanangeli, L. F. Bliven, and O. Le Calve, "A wind wave tank study of the azimuthal response of a Ka-band scatterometer," *IEEE Trans. Geosci. Remote Sensing*, vol. 29, pp. 143–148, Jan. 1991.

[27] M. R. Keller, W. C. Keller, and W. J. Plant, "A wave-tank study of the dependence of x-band cross sections on wind speed and water temperature," *J. Geophys. Res.*, vol. 97, no. C4, pp. 5771–5792, 1992.

[28] N. Ebuchi, H. Kawamura, and Y. Toba, "Physical processes of microwave backscattering from laboratory wind-wave surfaces," *J. Geophys. Res.*, vol. 98, no. C8, pp. 14 669–14 681, 1993.

[29] M. R. Keller, B. L. Gotwols, W. J. Plant, and W. C. Keller, "Comparison of optically-derived spectral densities and microwave cross-sections in a wind-wave tank," *J. Geophys. Res.,* vol. 100, no. C8, pp. 16 163–16 178, 1995.

[30] M. Coantic and A. Favre, "Activities in and preliminary results of air-sea interaction research at I.M.S.T.," *Adv. Geophys.*, vol. 16, pp. 391–405, 1974.

[31] L. F. Bliven and G. Norcross, "Effects of rainfall on scatterometer derived wind-speeds," in *Proc. Int. Geosci. Remote Sensing Symp.'88*, Eur. Space Agency, Edinburgh, Scotland, Sept. 12–16, 1988, vol. 1, ESA SP-284, pp. 565–566.

[32] H. Branger, A. Ramamonjiarisoa, and L. F. Bliven, "A ku-band laboratory experiment on the electromagnetic bias," *IEEE Trans. Geosci. Remote Sensing*, vol. 31, pp. 1165–1179, Nov. 1993.

[33] L. C. Schroeder, W. L. Jones, P. R. Schaffner, and J. L. Mitchell, "Flight measurements and analysis of AAFE Radscat wind speed signature of the ocean," NASA, Washington DC, Tech. Memo. 85646, 1984.

[34] R. E. Davis and L. A. Regier, "Methods for estimating directional wave spectra from multi-element arrays," *J. Marine Res.*, vol. 35, pp. 453–477, 1977.

[35] E. R. Jefferys, G. T. Waterman, M. Ramsden, and M. J. Platts, "Measuring directional spectra with the MLM," in *Proc. Directional Wave Spectra Appl. Conf.*, Univ. Calif., Los Angeles, 1981, pp. 203–219.

[36] M. Isobe, K. Kondo, and H. Horikawa, "Extension of MLM for estimating directional wave spectrum," in *Proc. Symp. Description*

Modeling Directional Seas, Tech. Univ., Lyngby, Denmark, 1984, vol. A6, pp. 1–15.
[37] M. A. Arribas and J. J. Egozcue, "Normalized maximum-likelihood estimators of the directional wave spectrum," *J. Atmos. Ocean. Technol.*, vol. 12, pp. 668–673, 1995.
[38] B. Jahne and K. S. Riemer, "Two-dimensional wave number spectra of small-scale water surface waves," *J. Geophys. Res.*, vol. 95, no. C7, pp. 11 531–11 546, July 1990.
[39] D. Van Haselma, C. Calkoen, W. A. Oost, P. Snoeij, J. Vogelzang, and B. Jahne, "Comparisons of backscattering calculations with measurements made in a large wind-wave flume," in *Proc. Int., Geosci. Remote Sensing Symp.'92*. New York: IEEE, vol. 92.
[40] B. Jahne and H. Schultz, "Calibration and accuracy of optical slope measurements for short wind waves," in *Proc. SPIE, Opt. Air–Sea Interface: Theory Measure.*, 1992, vol. 1749.
[41] D. S. Kwoh and B. M. Lake, "The nature of microwave scattering from water waves," TRW Space Technol. Group, CA, Rep. 37564 6002-ut-00, 1984.
[42] C. Skandrani, C. Kharif, and J. P. Giovanangeli, "An analytical study of short wave modulation by oblique swell," in *Proc. 2nd Int. Conf. Air–Sea Interaction Meteorol. Oceanogr. Coastal Zone*, Lisbon, Portugal, Sept. 22–27, 1994, vol. 1, pp. 144–145,.
[43] A. A. Townsend, "Flow in a deep turbulent boundary layer over a surface distorted by water waves," *J. Fluid Mech.*, vol. 55, pp. 719–735, 1972.
[44] M. A. Donelan, "The effect of swell on the growth of wind-waves," in *Proc. Symp. Measuring Ocean Waves from Space,* R. C. Beal, Ed. *Johns Hopkins Tech. Digest 8*, pp. 18–24, 1987.
[45] C. Garret and J. Smith, "On the interaction between long and short surface waves," *J. Phys. Ocean.*, vol. 6, pp. 925–930, 1976.
[46] Y. Toba, M. Hatori, Y. Imai, and M. Tokuda, *Wave Dynamics and Radio Probing of the Ocean Surface*, O. M. Phillips and K. Hasselmann, Eds. New York: Plenum, 1986.
[47] D. Masson, "On the nonlinear coupling between swell and wind waves," *J. Phys. Ocean.*, vol. 23, pp. 1249–1258, 1993.
[48] K. D. Ruvinsky and G. I. Freydman, "On the generation of capillary-gravity waves by steep gravity waves," *Izvestyias Atmos. Ocean. Phys.*, vol. 17, p. 7, 1981.
[49] M. L. Banner and E. H. Fooks, "On the microwave reflectivity of small-scale breaking water wave," in *Proc. R. Soc. Lond. A*, 1985, vol. 399, pp. 93–109.
[50] M. S. Longuet-Higgins, "Capillary rollers and bores," *J. Fluid Mech.*, vol. 240, pp. 659–679, 1992.
[51] A. T. Jessup, W. K. Melville, and W. C. Keller, "Breaking waves affecting microwave backscatter—1: Detection and verification," *J. Geophys. Res.*, vol. 96, no. C11, pp. 20 547–20 559, 1991.
[52] ———, "Breaking waves affecting microwave backscatter—2: Dependence on wind and wave conditions," *J. Geophys. Res.,* vol. 96, no. C11, pp. 20 561–20 569, 1991.
[53] S. L. Durden and J. E. Vesecky, "A physical radar cross section model for a wind-driven sea with swell," *IEEE Trans. Oceanic Eng.*, vol. 10, pp. 445–451, 1985.